Research Square

Preprints are preliminary reports that have not undergone peer review.
They should not be considered conclusive, used to inform clinical practice,
or referenced by the media as validated information.

Core Activation Patterns Across Different Figure Skating Jumps

Pavla Nikelova
VSB—Technical University of Ostrava https://orcid.org/0009-0002-2832-005X
Vilem Hlavsa
University of Ostrava
Michal Magiera
VSB—Technical University of Ostrava https://orcid.org/0009-0005-7495-7969
Jaroslav Uchytil
University of Ostrava https://orcid.org/0000-0002-8108-6357
Martina Ladrova
VSB—Technical University of Ostrava https://orcid.org/0000-0002-5316-475X
Sarka Cenkova
VSB—Technical University of Ostrava https://orcid.org/0009-0001-0440-4403
Radek Martinek
VSB—Technical University of Ostrava https://orcid.org/0000-0003-2054-143X
Roman Vala
VSB—Technical University of Ostrava https://orcid.org/0000-0001-6713-225X
Tomas Rypar
VSB—Technical University of Ostrava https://orcid.org/0009-0008-7240-3833
Rene Jaros
rene.jaros@vsb.cz

VSB—Technical University of Ostrava https://orcid.org/0000-0003-3346-6467

Research Article

Keywords: figure skating, electromyography; inertial measurement units, wearable sensors, core muscle activation, takeoff and landing detection, jump phase segmentation

Posted Date: June 26th, 2026

DOI: https://doi.org/10.21203/rs.3.rs-10152476/v1

License: This work is licensed under a Creative Commons Attribution 4.0 International License.
Read Full License

Additional Declarations: The authors declare no competing interests.

Core Activation Patterns Across Different Figure Skating Jumps

Pavla Nikelova [1], Vilem Hlavsa[2], Michal Magiera [1], Jaroslav Uchytil [2], Martina Ladrova [1], Sarka Cenkova [1], Radek Martinek [1], Roman Vala [1], Tomas Rypar [1], and Rene Jaros [1]

[1]Department of Cybernetics and Biomedical Engineering, Faculty of Electrical Engineering and Computer Science, VSB—Technical University of Ostrava, 17. listopadu 2172/15, Ostrava, 708 00, Czechia
[2]Department of Human Movement Studies, Faculty of Education, University of Ostrava, Varenská 40a, Ostrava, 702 00, Czechia

June 25, 2026

Abstract

This study presents a quantitative analysis of core muscle activation patterns across six distinct figure skating jumps: single/double axel, double/triple salchow, and double/triple loop. While previous research has focused primarily on lower-limb kinematics, the role of the trunk in maintaining a rigid rotational axis remains underexplored. We utilized a synchronized sensor framework comprising torso-mounted accelerometers, bilateral electromyography (EMG) of the m. obliquus externus abdominis and m. rectus abdominis, and skate-mounted inertial measurement units to monitor 12 adolescent female athletes. The EMG signals were segmented into the preparation, flight, and landing phases and subsequently normalized to the percentage of inter-trial maximum (%ITM). Our findings reveal a consistent shift from right-side dominance during the preparation phase to left-side dominance during the flight phase (for counter-clockwise rotators). Triple jumps exhibited significantly higher integrated ITM in the obliquus externus compared to double jumps, despite minimal differences in airtime. This suggests that increased rotational velocity (≈1570 °/s) necessitates higher muscular tension rather than a longer duration in the air. Furthermore, the landing phase was characterized by a powerful bracing mechanism, with the co-contraction index exceeding 80% in high-rotation jumps. This study provides an objective framework for evaluating jump technique and optimizing strength training in competitive figure skating.

Keywords figure skating; electromyography; inertial measurement units; wearable sensors; core muscle activation; takeoff and landing detection; jump phase segmentation.

1 Introduction

The biomechanical complexity of figure skating jumps requires precise coordination of rotational momentum, explosive power, and mid-air stability. Recent advancements in sports science have shifted from subjective judging toward objective quantification using wearable sensors: electromyography (EMG), inertial measurement units (IMUs) and high-speed motion analysis. This research explores the multimodal quantitative analysis of jump execution, focusing on core coordination and activation.

A critical challenge in modern figure skating is the accurate classification and measurement of technical elements. Moessing et al. [1] demonstrated that the placement of IMUs is crutial, with the identification of the ankles as the optimal site for achieving classification precisions exceeding 98%. Furthermore, the precision of vertical jump measurement has been significantly enhanced by wearable systems incorporating

laser Time-of-Flight sensors, which achieve up to 99% accuracy in height detection (Panfili et al.[2]). The practicality of using single-unit wearable sensors to monitor complex on-ice motions is well established. Bruening et al. [3] demonstrated that IMUs can reliably capture critical flight parameters such as peak rotation speeds generally up to 1,500 °/s (with absolute peaks reaching 1,665 °/s) and accurately estimate flight time and jump height with errors under 7% and 15% respectively.

The transition from single to multi-rotational jumps imposes extreme demands on the musculoskeletal system. Research by Pantoja et al. [4] indicates that higher-order jumps (e.g., double axels) require significantly longer and more intense muscle activation, particularly in the gluteal and quadriceps groups during the takeoff and flight phases. Koga et al. [5] also demonstrated that as jump difficulty increases, figure skaters rely on significantly greater hip flexion during propulsion and elevated muscular activation of the hamstrings, quadriceps, and tibialis anterior. The role of the trunk is equally crucial. Yamaguchi and Sakurai [6] found that while limb swing patterns vary across the six jump types, the trunk consistently generates a large local angular momentum as the central axis for rotation. Successfully completing multi-rotational jumps requires vast control over this axis during the flight phase. Kinematic analysis by Shi et al. [7] revealed that athletes struggle significantly more to maintain a minimized moment of inertia as jump revolutions increase. The overcome theoretically demands intense activation of the trunk musculature to lock the body into a rigid rotational axis. Bingül et al. [8] supported that an off-ice core training program significantly altered lower-extremity kinematics, narrowing the knee exit angle to effectively transfer horizontal momentum into vertical jump height. However, direct EMG quantification of the core during these phases remains underexplored.

The quality of execution is often determined by the skater's ability to maintain a rigid vertical axis and stable landing against intense physical impact. Hara et al. [9] mapped the extreme three-dimensional ground reaction forces and moments applied to the skate blade during critical transition periods of takeoff and landing. The core muscles must provide dynamic stabilization to neutralize these forces. Biomechanical modeling by Han Li [10] highlights that landing stability is linked to strict hip-knee coordination, with instability in the hip joint often leading to technical deviations. Mastering this precise multi-joint coordination remains a critical focus for both on-ice technical development and biomechanical evaluation. Helesic and Lehnert [11] showed that lower-limb explosive strength and specific velocity are strong predictors of judges' scores and overall competition success. Furthermore, comprehensive off-ice training that includes targeted stretching routines has been proven to assist lower extremity coordination and significantly improve explosive takeoff power (Mochida et al. [12]). Rapid mechanical changes in movement are difficult to assess with the naked eye. Hirosawa et al. [13] demonstrated that combining precise kinematic tracking with the visual patterns of figure skating specialists can effectively evaluate execution quality. Although spectators often emphasize the physical parameters of a jump, such as raw height and flight time, evidence suggests that the scoring of judges is actually more closely correlated with horizontal distance and the ratio of height to length (Hirosawa et al. [14]).

By synthesizing the aforementioned findings and addressing the underexplored gap in direct core quantification, this study aims to analyze the association between internal muscle activation patterns and external kinematic outcomes across various figure skating jumps. To achieve this, we used data from a portable system with an accelerometer (ACC) and surface EMG sensors to monitor trunk dynamics and core muscle activation. In addition, two IMUs were used to measure rotational velocity and flight time. Ultimately, this approach provides new objective insights into the biomechanics of figure skating and demonstrates a framework that could be used to evaluate jump technique and optimize training.

The following part of the study is divided into methodology 2, results 3, discussion 4 and conclusion 5, and its main contributions are:

- Own publicly available figure skating dataset with annotations, including recordings of 12 (adolescent) female participants. Including 2 or 4 EMG and ACC data records, distinguishing 6 types of jumps, with additional information from the Aiving IMU device.
- Creation of jump phases annotations through multimodal data analysis assessment of takeoff, airtime

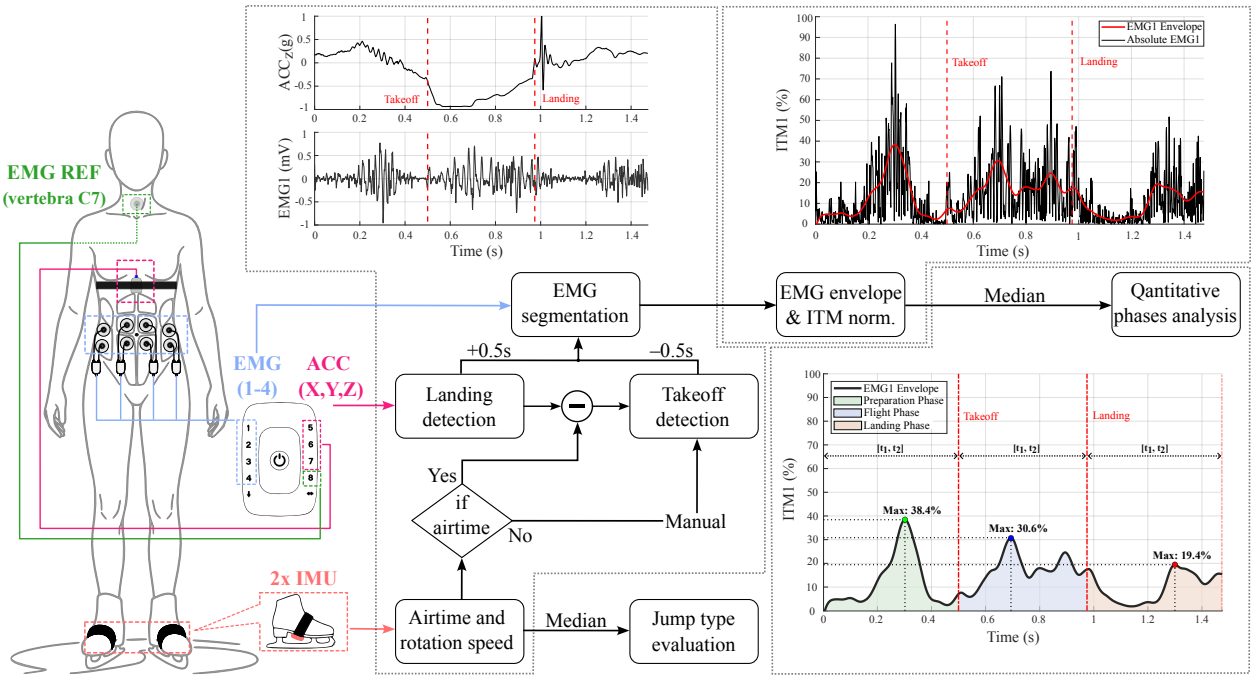


Figure 1: Flowchart diagram of the methodology and signal processing, with signal visualizations from subject 1 (jump type 1A, obliquus externus sinister muscle - EMG1, first trial).

and landing moments using ACC and IMU data (or manually when airtime unavailable) with following synchronization and analysis of these time phases within core muscles EMG data.

- Quantitative evaluation of EMG signals, specifically activation levels, timing, and muscular symmetry of the right and left side core muscles (m. rectus abdominis dexter et sinister and m. obliquus externus dexter et sinister) in 6 different types of jump within its three phases (preparation, airtime, landing).
- Quantitative analysis and comparison of airtime and rotation speed in 6 different jump types.

2 Methodology

The methodological framework of this study followed a structured sequence of data acquisition, signal processing, and quantitative evaluation, as illustrated in the experimental workflow in Fig. 1. This process integrated synchronized biomechanical and physiological measurements to capture the complex dynamics of figure skating jumps, ensuring high data fidelity from initial sensor placement to the final statistical analysis.

2.1 Subjects and Sensors

The study sample consisted of 12 female participants in the age group of adolescents. The descriptive statistics for the cohort are summarized in Tab. 1. The study was conducted strictly in accordance with ethical standards. Formal approval was granted by the institutional Ethics Committee of the University of Ostrava, under the reference number OU-13799/45-2026. Prior to the commencement of the research, informed consent was obtained from all participants (and their legal guardians, where applicable), ensuring that they were fully aware of the nature of the study, data handling procedures and their right to withdraw at any time.

The experimental setup utilized a synchronized multi-sensor approach to capture the biomechanical and

physiological demands of figure skating maneuvers. A torso-mounted ACC sensor (3 ACC channels, one for each axis) and up to 4 bipolar electromyography sensors with one common reference electrode (resulting in at most 4 EMG channels) were used to monitor trunk dynamics and core muscle activation patterns, both recorded at a sampling frequency of 1000 Hz, using the portable Plux Biosignals system (8-Channel biosignalsplux Kit) with 16-bit resolution per channel, wirelessly connected to the native OpenSignals software. The measured muscles were m. rectus abdominis dexter et sinister and m. obliquus externus dexter et sinister. In the initial phase of the study (for the first 6 subjects), EMG signals were recorded for the right and left external oblique muscles. Following an initial evaluation and confirmation of the correct methodological procedure, measurements of the right and left rectus abdominis muscles were added for the following 6 subjects. The reference electrode was placed on the seventh cervical vertebra (C7). Simultaneously, two Aiving Jump Tracker (IMU) sensors were positioned on the athlete's skates (one per leg) to wirelessly track precise movement dynamics, using a native app, specifically measuring rotation speed and airtime. This dual sensor approach ensures that the moment of final contact with the ice surface during takeoff and the moment of first contact upon landing are captured, regardless of whether the contact is made by the right or left lower limb. For consistency across the sample, all jumps were performed with a counter-clockwise rotation (leftward). The following jumps were distinguished by their takeoff mechanics, specifically noting the launch direction and whether the skate blade leans inward (inner edge) or outward (outer edge). Additionally, because all standard jumps land backward, the forward-takeoff axel inherently requires an extra half-rotation:

- **Single axel (1A):** Forward takeoff (outer edge), 1.5 airborne rotations.
- **Double axel (2A):** Forward takeoff (outer edge), 2.5 airborne rotations.
- **Double salchow (2S):** Backward takeoff (inner edge), 2 airborne rotations.
- **Triple salchow (3S):** Backward takeoff (inner edge), 3 airborne rotations.
- **Double loop (2LO):** Backward takeoff (outer edge), 2 airborne rotations.
- **Triple loop (3LO):** Backward takeoff (outer edge), 3 airborne rotations.

Data were collected during the execution of a specific jumping battery. The exact composition and the final number of records depended on the physical ability of the individual participants to perform the given type of jump and the number of repetitions (see Tab. 1).

Table 1: Subject characteristics and jump battery specifications.

Subj. ID	**Age (yrs)**	**Hgt. (cm)**	**Wgt. (kg)**	**BMI (-)**	**1A (n)**	**2A (n)**	**2S (n)**	**3S (n)**	**2LO (n)**	**3LO (n)**
1	19	159	53.0	21.0	6	3	5	0	5	0
2	16	157	62.1	25.2	6	4	3	5	0	0
3	13	162	44.5	17.0	6	6	6	6	0	0
4	13	152	42.2	18.3	6	6	0	0	0	0
5	13	164	49.0	18.2	6	5	0	0	6	5
6	13	157	44.5	18.1	6	6	6	1	0	0
7	14	155	39.0	16.2	6	6	6	6	6	6
8	16	163	48.0	18.1	6	6	6	6	6	6
9	17	168	54.0	19.1	6	6	6	6	6	0
10	15	163	52.0	19.6	6	6	6	4	6	6
11	18	167	55.0	19.7	6	6	6	6	6	6
12	17	172	54.7	18.5	6	6	6	5	0	0
Mean	15.3	161.6	49.83	19.07	6.00	5.50	4.67	3.75	3.42	2.42
Sum	-	-	-	-	72	66	56	45	41	29

2.2 Data processing

The raw data underwent a processing pipeline to ensure consistency between the recorded sessions. The detection of takeoff and landing was mainly facilitated by the Aiving IMU. First, the landing was identified from the Z-axis of the ACC data (first peak before global maximum), from which the airtime (from Aiving IMU) was subtracted to determine the takeoff. In cases where automated airtime data from Aiving was unavailable due to native algorithm segmentation failures during non-standard or atypical jump execution profiles, the takeoff was manually detected based on ACC signal morphology and time estimation. Following the methodology of previous studies [15, 16, 17], the EMG signals were segmented into three distinct phases (preparation, flight, and landing) defined within a window starting 0.5 s before takeoff and ending 0.5 s after landing. Data processing and analysis were conducted using MATLAB R2023a (MathWorks, Natick, MA, USA). To facilitate comparison across trials and subjects, each of these functional phases underwent time-normalization, being resampled to 500 samples to account for variations in jump duration (jump phase lasted from 450 to 580 ms). Subsequently, the EMG envelope was calculated from the absolute value of EMG (positive values) using the 4th order low-pass Butterworth filter with cutoff frequency of 6 Hz and normalized to the percentage of inter-trial maximum (%ITM), where 100% was defined as the absolute maximum value achieved across all six trials for a given difficulty (e.g., pooling 1A and 2A together to establish a stable baseline). This identical normalization approach was applied to all other jump types. [18].

2.3 Methods of Data Analysis

The final stage of the methodology used a quantitative data analysis to evaluate the performance of the athlete. Through discrete analysis, specific biomechanical and physiological metrics were extracted, including peak inter-trial maximum (PITM), PITM time, and integrated ITM (IITM), along with rotation speed and airtime derived from the Aiving IMU or accelerometer. All calculated parameters were independently analyzed for each jump phase. Specifically, these metrics were first computed individually for each trial and each jump of every subject. To aggregate the data, the median was calculated in all trials for each subject and subsequently the overall median was determined across the entire cohort of subjects.

2.3.1 Muscle Activity and Timing

The time of peak inter trial maximum (PITM Time) in seconds was calculated by converting the sample index based on the sampling frequency 1000 Hz. Crucially, this calculation was performed using non-normalized time series data, meaning that the resulting time is absolute and relative to the onset (zero-point) of each specific jump phase (preparation, flight, or landing).

The IITM represents the area under the ITM envelope (ITM) within the time interval of a specific phase $[t_1, t_2]$ [19, 16]:

$$IITM = \int_{t_1}^{t_2} ITM(t)\, dt. \tag{1}$$

2.3.2 Co-contraction Index (CCI)

To evaluate muscular symmetry and the degree of simultaneous activation between the left (L) and right (R) sides of the trunk, a Co-contraction Index (Symmetry Index) was utilized [20]. This parameter was calculated for both peak amplitude (CCIP) and the total muscle work (CCII):

$$CCIP = \left(\frac{\min(PITM_L, PITM_R)}{\max(PITM_L, PITM_R)} \right) \cdot 100\,(\%), \tag{2}$$

$$CCII = \left(\frac{\min(IITM_L, IITM_R)}{\max(IITM_L, IITM_R)} \right) \cdot 100\,(\%). \tag{3}$$

Table 2: Jump phase parameters for left (EMG1) and right (EMG2) obliquus sides.

Jump	Phase	Left Side (EMG1)			Right Side (EMG2)		
		PITM (%)	PITM Time (s)	IITM (-)	PITM (%)	PITM Time (s)	IITM (-)
1A	Preparation	**49.4** (40.6–64.1)	**0.330** (0.308–0.366)	**10223** (8107–11503)	**66.9** (49.2–76.9)	**0.424** (0.402–0.429)	**11573** (8646–12403)
	Flight	**72.6** (40.7–79.8)	**0.344** (0.179–0.404)	**16966** (9885–18675)	**40.4** (23.5–46.0)	**0.190** (0.132–0.384)	**8757** (5339–9981)
	Landing	**39.3** (29.2–43.6)	**0.261** (0.069–0.420)	**10319** (6508–11617)	**42.8** (25.6–55.4)	**0.039** (0.022–0.077)	**7267** (5518–8062)
2A	Preparation	**48.6** (32.2–60.3)	**0.320** (0.306–0.371)	**9930** (7262–11364)	**59.8** (42.7–74.7)	**0.400** (0.364–0.448)	**9953** (8182–13998)
	Flight	**74.9** (71.4–78.4)	**0.416** (0.351–0.441)	**16992** (12732–22047)	**50.0** (40.7–63.6)	**0.204** (0.071–0.340)	**12495** (9030–15852)
	Landing	**38.1** (29.1–50.8)	**0.051** (0.006–0.168)	**7108** (5362–10839)	**46.0** (35.1–56.3)	**0.058** (0.025–0.112)	**7429** (6371–8840)
2S	Preparation	**26.2** (16.0–31.0)	**0.403** (0.360–0.427)	**6064** (2699–7767)	**55.4** (19.4–78.2)	**0.438** (0.420–0.456)	**9207** (2307–13564)
	Flight	**62.8** (37.3–70.9)	**0.425** (0.326–0.524)	**11545** (3923–15438)	**45.5** (32.0–54.7)	**0.344** (0.086–0.524)	**5260** (4278–6311)
	Landing	**47.7** (35.7–71.6)	**0.041** (0.024–0.292)	**7383** (6053–8891)	**55.7** (15.6–83.8)	**0.038** (0.018–0.047)	**5733** (3718–6846)
3S	Preparation	**24.2** (12.8–28.7)	**0.401** (0.358–0.460)	**6172** (3955–8002)	**56.4** (30.6–83.2)	**0.411** (0.355–0.461)	**10885** (5196–16162)
	Flight	**80.1** (52.9–84.4)	**0.452** (0.385–0.529)	**14833** (4495–17564)	**55.3** (40.9–73.0)	**0.456** (0.226–0.525)	**11090** (6759–15095)
	Landing	**46.7** (35.3–79.6)	**0.039** (0.025–0.256)	**8174** (6944–9255)	**55.0** (41.4–78.5)	**0.063** (0.023–0.090)	**7079** (5550–10196)
2LO	Preparation	**52.7** (23.4–57.1)	**0.487** (0.370–0.499)	**10293** (3801–12372)	**58.6** (29.1–68.7)	**0.398** (0.278–0.460)	**11980** (4719–14049)
	Flight	**81.1** (48.9–88.2)	**0.344** (0.264–0.438)	**17060** (6052–22061)	**46.4** (35.5–54.2)	**0.215** (0.080–0.383)	**6234** (4298–9216)
	Landing	**44.2** (31.2–85.2)	**0.037** (0.028–0.153)	**6943** (6613–9518)	**27.3** (17.6–82.4)	**0.035** (0.030–0.043)	**4857** (3178–8020)
3LO	Preparation	**27.2** (18.5–48.7)	**0.448** (0.261–0.469)	**7375** (4550–11693)	**73.0** (57.8–89.7)	**0.244** (0.209–0.368)	**16303** (12429–17744)
	Flight	**80.4** (59.4–83.3)	**0.451** (0.415–0.492)	**13752** (8766–18494)	**45.9** (41.7–73.2)	**0.428** (0.282–0.497)	**10878** (9301–14674)
	Landing	**40.7** (34.4–92.5)	**0.013** (0.000–0.112)	**6456** (6082–8221)	**28.6** (27.5–77.2)	**0.074** (0.025–0.083)	**5945** (5370–6587)

Note: Values are represeted as: median (25th percentile - 75th percentile).

A CCI value = 100% indicates perfect bilateral symmetry in muscle activation, while lower values suggest the dominance of one side (lateralization) during movement.

3 Results

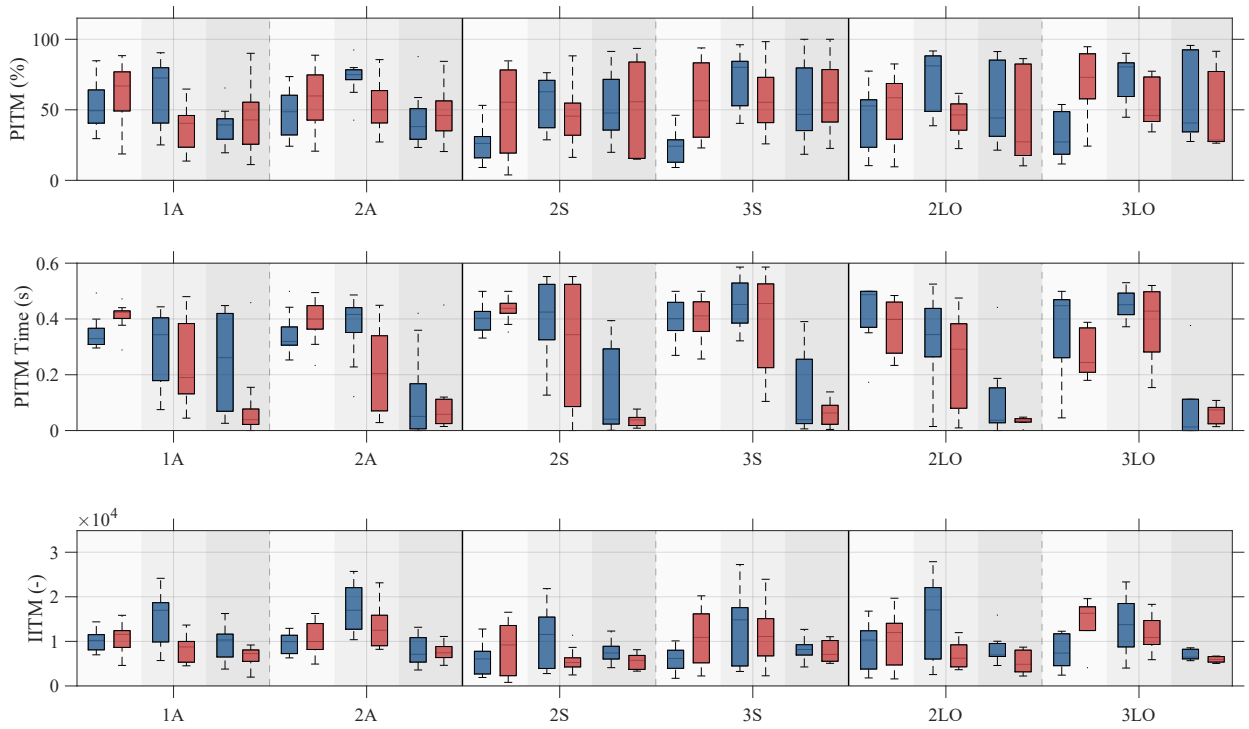
The neuromuscular and kinematic parameters of the abdominal wall were evaluated in various figure skating jumps to map core stabilization strategies. The experimental design focused on tracking the mechanical and electrical behavior of the trunk musculature during distinct execution phases: preparation, flight, and landing. Through the integration of EMG metrics and kinematic data, the analysis identifies how specific jump entries, rotational demands, and impact forces modulate core recruitment.

To provide a comprehensive overview of the control mechanisms, the findings are structured into specialized subsections. First, the bilateral lateralization patterns of the individual muscles are examined in Section 3.1. Furthermore, the specific modifications imposed by directional entry constraints and takeoff variations are detailed in Section 3.2. The mechanical scaling of the core due to the increase in rotational velocity is evaluated in Section 3.3. Finally, Section 3.4 contextualizes these neuromuscular profiles by establishing their direct relationship with kinematic baselines, specifically rotation speed and air time.

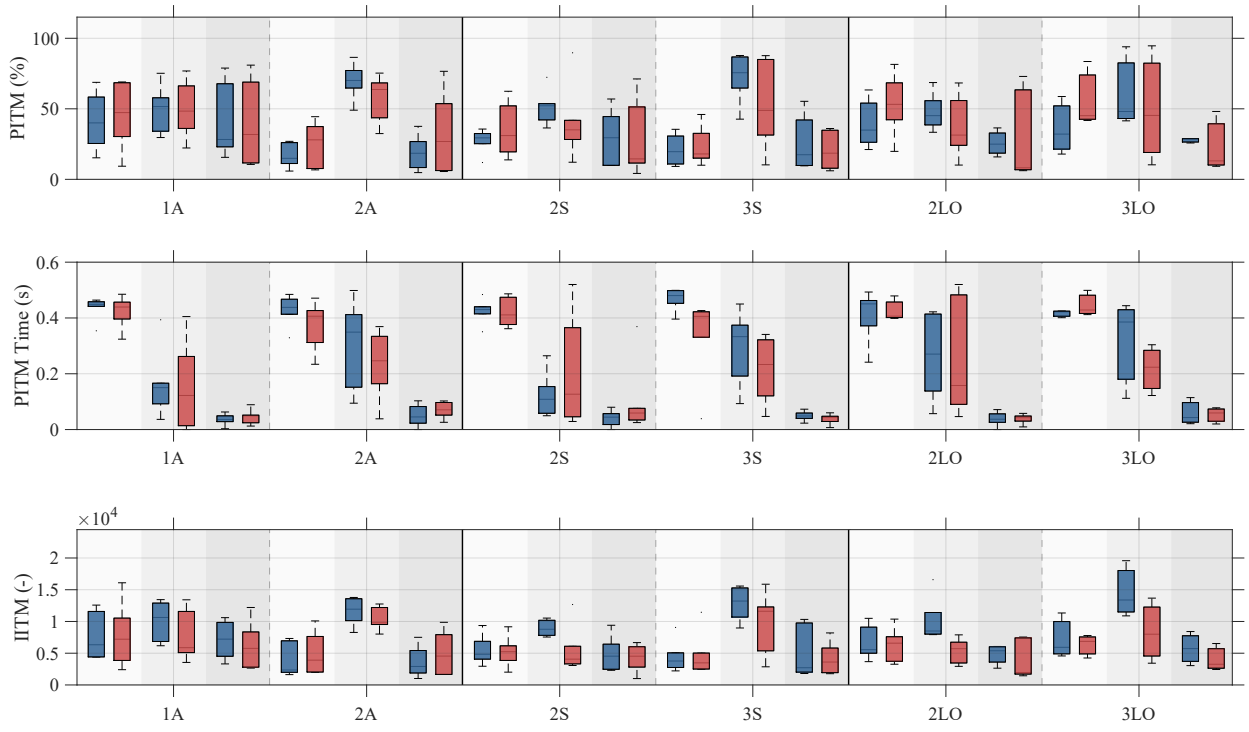
3.1 Bilateral Asymmetry of Trunk Muscle Activity (Left vs. Right)

To evaluate neuromotor control strategies during figure skating jumps, unilateral muscle activity and bilateral symmetry were assessed by comparing the left and right sides of the m. obliquus externus abdominis (EMG1 vs. EMG2) and m. rectus abdominis (EMG3 vs. EMG4). The data revealed substantial bilateral asymmetries across almost all jump types, depending on the specific jump phase (preparation, flight, and landing), as visually summarized in the boxplot distributions (Fig. 2a and Fig. 2b).

The obliquus muscle group demonstrated highly lateralized activation patterns, particularly during the preparation and flight phases, as detailed in Tab. 2. During the preparation phase, a pronounced dominance of the right-side was observed on nearly all jumps. The most notable asymmetry occurred during 3LO, where the right side (EMG2) reached an IITM of 16303 (12429–17744), whereas the left side (EMG1) reached less than half that value at 7375 (4550–11693). This asymmetry also confirms a CCII value of 61.6%. At the



(a) obliquus EMG parameters: Left vs. Right side.



(b) rectus EMG parameters: Left vs. Right side.

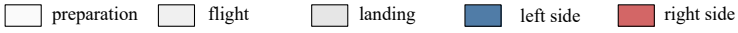


Figure 2: Comprehensive evaluation of core muscle activation parameters across different figure skating jumps.

Table 3: Obliquus coactivation median values (%) for CCIP and CCII across different jumps and phases.

Jump	**Phase**	**CCIP (%)**	**CCII (%)**
1A	Preparation	68.9	75.9
	Flight	57.1	51.8
	Landing	61.1	61.7
2A	Preparation	58.9	76.0
	Flight	71.6	72.4
	Landing	62.1	62.8
2S	Preparation	52.6	69.7
	Flight	77.2	61.9
	Landing	62.4	88.0
3S	Preparation	42.5	56.7
	Flight	60.0	60.0
	Landing	60.6	69.6
2LO	Preparation	82.1	82.1
	Flight	65.8	42.8
	Landing	63.9	72.6
3LO	Preparation	52.5	61.6
	Flight	64.6	71.4
	Landing	71.7	88.2

Table 4: Jump phase parameters for left (EMG3) and right (EMG4) rectus sides.

Jump	**Phase**	**Left Side (EMG3)**			**Right Side (EMG4)**		
		PITM (%)	**PITM Time (s)**	**IITM (-)**	**PITM (%)**	**PITM Time (s)**	**IITM (-)**
1A	Preparation	**40.0** (25.4–58.3)	**0.449** (0.442–0.458)	**6331** (4426–11576)	**47.3** (30.3–68.4)	**0.439** (0.397–0.457)	**7205** (3864–10520)
	Flight	**51.6** (34.1–57.8)	**0.150** (0.092–0.166)	**10631** (6847–12886)	**48.4** (36.1–66.2)	**0.122** (0.014–0.262)	**5872** (5099–11577)
	Landing	**28.3** (23.1–67.7)	**0.036** (0.029–0.049)	**7217** (4525–9849)	**31.8** (11.7–68.9)	**0.049** (0.025–0.051)	**5762** (2803–8341)
2A	Preparation	**14.9** (11.2–26.0)	**0.438** (0.413–0.467)	**2356** (1994–6944)	**28.0** (7.7–37.4)	**0.406** (0.312–0.426)	**3905** (2042–7636)
	Flight	**70.1** (64.8–77.2)	**0.349** (0.152–0.412)	**11937** (10138–13575)	**63.7** (43.7–68.3)	**0.246** (0.165–0.334)	**9793** (9521–12199)
	Landing	**18.5** (8.4–26.8)	**0.045** (0.023–0.083)	**2914** (1895–5427)	**26.8** (6.2–53.6)	**0.071** (0.052–0.097)	**4548** (1661–7916)
2S	Preparation	**29.4** (25.3–32.5)	**0.430** (0.415–0.440)	**4834** (4073–6867)	**31.0** (19.5–52.0)	**0.411** (0.377–0.474)	**5240** (3861–6156)
	Flight	**52.2** (42.2–53.7)	**0.108** (0.059–0.154)	**8773** (7813–10180)	**35.1** (28.3–41.8)	**0.127** (0.046–0.365)	**4066** (3329–6088)
	Landing	**29.5** (9.9–44.5)	**0.044** (0.018–0.057)	**4535** (2477–6415)	**14.5** (11.6–51.3)	**0.059** (0.035–0.076)	**4530** (2823–6018)
3S	Preparation	**19.6** (10.9–30.6)	**0.480** (0.453–0.498)	**3771** (2753–5049)	**18.0** (15.1–32.6)	**0.406** (0.331–0.422)	**3479** (2516–5012)
	Flight	**75.6** (64.8–86.7)	**0.333** (0.192–0.374)	**13215** (10700–15274)	**48.9** (31.5–85.0)	**0.233** (0.121–0.321)	**11610** (5385–12279)
	Landing	**17.4** (9.8–42.0)	**0.049** (0.040–0.059)	**2714** (2026–9752)	**18.5** (7.9–34.8)	**0.044** (0.029–0.048)	**3609** (1941–5803)
2LO	Preparation	**34.9** (26.3–54.0)	**0.451** (0.372–0.463)	**5557** (5005–9097)	**53.2** (42.3–68.4)	**0.406** (0.402–0.457)	**6581** (3732–7588)
	Flight	**45.2** (38.6–55.7)	**0.271** (0.138–0.414)	**8498** (8015–11413)	**31.4** (24.1–55.9)	**0.158** (0.090–0.482)	**5710** (3472–6725)
	Landing	**25.0** (18.6–32.8)	**0.037** (0.026–0.056)	**5383** (3615–6009)	**8.2** (6.8–63.4)	**0.043** (0.030–0.048)	**1964** (1721–7409)
3LO	Preparation	**32.1** (21.5–52.1)	**0.422** (0.406–0.424)	**5930** (4909–9986)	**45.1** (42.6–73.9)	**0.428** (0.416–0.481)	**6866** (4901–7554)
	Flight	**48.1** (43.1–82.5)	**0.386** (0.180–0.429)	**13382** (11508–18025)	**45.3** (19.1–82.3)	**0.224** (0.147–0.284)	**7994** (4568–12257)
	Landing	**28.6** (26.5–28.8)	**0.043** (0.026–0.097)	**5725** (3715–7741)	**13.1** (10.2–39.4)	**0.059** (0.030–0.073)	**3260** (2644–5709)

Note: Values are represented as: median (25th percentile - 75th percentile).

Table 5: Rectus coactivation median values (%) for CCIP and CCII across different jumps and phases.

Jump	Phase	CCIP (%)	CCII (%)
1A	Preparation	55.9	61.1
	Flight	56.2	66.1
	Landing	77.4	66.3
2A	Preparation	67.4	69.6
	Flight	75.5	81.5
	Landing	60.8	55.4
2S	Preparation	60.5	61.5
	Flight	66.6	48.7
	Landing	52.2	57.7
3S	Preparation	40.1	59.2
	Flight	60.0	75.6
	Landing	54.8	54.2
2LO	Preparation	75.0	79.7
	Flight	61.9	54.9
	Landing	35.8	47.4
3LO	Preparation	70.3	66.0
	Flight	46.4	46.5
	Landing	49.2	51.2

same time, the PITM shifted toward the very end of the phase (0.448 s) on the left side (27.2%), while the right side peaked much earlier (73.0%) at 0.244 s. A similar preparatory pattern was evident in the 3S, where the right-side obliquus displayed a higher PITM (56.4% vs. 24.2%). This collective behavior points to a strong eccentric pre-activation and unilateral rotational role of the right oblique musculature immediately prior to takeoff.

In contrast to the preparation phase, the flight phase was characterized by a shift toward left-side dominance in edge-rotational jumps. During 2S, PITM reached 62.8% on the left side but only 45.5% on the right side. This left-sided dominance was amplified in multi-rotational types, such as the 3S, where left-side PITM reached its highest value at 80.1% compared to 55.3% on the right, accompanied by a markedly higher IITM (14833 vs. 11090). This lateralization is also confirmed by CCIP values of 77.2% for 2S and 60.0% for 3S. This reflects the unilateral technical demands of generating and maintaining core tightness during rapid air rotation.

The rectus muscle exhibited a different asymmetry profile (Tab. 4), functioning primarily as a central sagittal stabilizer. In contrast to the oblique musculature, the rectus abdominis demonstrated its highest level of bilateral symmetry and coactivation during the flight phase across nearly all jump types, as supported by the elevated coactivation indices in Tab. 5. This synchronous behavior is particularly evident in multi-rotational types such as the 2A, where bilateral coactivation peaked at a CCIP of 75.5% and a CCII of 81.5%. Although the left rectus (EMG3) reached a slightly higher IITM of 11937 (10138–13575) compared to the right side (EMG4) at 9793 (9521–12199), the peak activation (PITM) remained closely balanced between the sides (70.1% left vs. 63.7% right). This strong in-flight symmetry underlines the muscle's role as a solid central pillar maintaining body alignment along the rotational axis.

The bilateral neuromuscular behavior during the landing phase was highly distinct between the two muscle groups and strictly dependent on the specific jump type. The lateral oblique walls demonstrated a powerful highly synchronized bilateral bracing mechanism to stabilize the vertical axis against intense rotational

momentum, especially during triple jumps, where obliquus coactivation reached its maximum during the landings of the 3S (69.6% CCII) and the 3LO (88.2% CCII, Tab. 5). This intense symmetrical coupling in the 3LO was driven by an ultra-rapid left-side obliquus onset peaking at just 0.013 s with an IITM of 6456 (Tab. 2). In contrast, the rectus abdominis functioned through a much more lateralized and asymmetric profile during landing (Tab. 5). During the 3LO landing, rectus coactivation decreased to 51.2% CCII, with left-side activity nearly doubled on the right side (left IITM: 5725, PITM: 28.6% vs. right IITM: 3260, PITM: 13.1%, Tab. 4). On the other hand, during the axel and salchow landings, the rectus symmetry profile shifted. The 1A landing was characterized by a sagittal bracing index of 77.4% CCIP, whereas during the 2A landing, a delay occurred on the right-side, the PITM Time shifted significantly to 0.071 s compared to 0.045 s on the left side.

In summary, the data demonstrate a distinct phase-dependent lateralization. The oblique muscles transition from right-side dominance during preparation to left-side dominance during flight, while the rectus muscle shifts from a synchronous in-flight coactivation profile to a phase-specific and jump-specific activation distribution during landing. This quantifies a highly coordinated asymmetric neuromuscular framework underlying complex rotational figure skating elements.

3.2 Influence of takeoff Mechanics (Axel vs. Salchow vs. Loop)

The structural differences in takeoff mechanics between the axel, salchow, and loop jumps noticeably influence the muscular activation of the abdominal core during the preparation phase. The primary distinction lies in the direction of the takeoff, where the axel is executed from a forward edge, while the salchow and loop are launched from a backward edge, requiring different stabilization strategies from the obliquus and rectus muscles.

For axel jumps, forward takeoff demands a highly balanced bracing strategy to convert linear momentum into vertical lift. As detailed in Tab. 2 and Tab. 4, the preparation phase of the double axel shows remarkably symmetric timing and integrated activity between both sides. The left obliquus displays an IITM of 9930 and the right side shows 9953, while the rectus muscle maintains a similar balanced activation profile (IITM left 2356 and IITM right 3905). This uniform tension across the entire abdominal wall supports a linear symmetric projection into the air, minimizing early asymmetric rotational torque before the skater leaves the ice.

In contrast, edge jumps initiated from a backward position introduce strong bilateral asymmetries and higher overall activation to initiate or control rotation. The loop jump, characterized by the takeoff from a crossed-foot position, exhibits the most intense preparatory muscle contraction. In the 2LO preparation, the obliquus muscle reaches its highest coactivation levels in the study, with a CCIP of 82.1%, reflecting a powerful tightening of the muscular belt to resist axial forces. When advancing to the triple loop, this mechanism becomes highly lateralized, with the right obliquus reaching an extreme IITM of 16303 compared to only 7375 on the left side. This sharp asymmetry indicates that the right lateral wall acts as the primary driver for winding up the torso.

The salchow jump utilizes a different mechanical approach from the loop, relying more on the swing of the free leg and less on the maximum isometric trunk tension. Consequently, the preparation phases for 2S and 3S show much lower coactivation values for both obliquus and rectus muscles (for 2S: CCIP 52.6% for the obliquus and CCIP 60.5% for the rectus). However, the salchow displays a unique lateralization in the peak of muscle activity within the preparation phase. During the 3S, the left obliquus reaches its maximum activity of 24.2%, while the right side reaches its maximum of 56.4%.

3.3 Influence of Rotational Velocity (Double vs. Triple Jumps)

Increasing the number of revolutions from double to triple jumps (single to double) fundamentally intensifies both overall muscular recruitment (IITM) and phase-specific coactivation (CCI), while altering peak activation strategies.

During the preparation phase, advancing from double to triple edge jumps leads to an explosive increase in unilateral torque. In the loop, the right obliquus IITM surges from 11980 in the 2LO to an extreme 16303 in the 3LO, maximizing rotational activation. In contrast, salchow shifts towards kinetic efficiency; the obliquus coactivation actually drops from 52.6% in the 2S to 42.5% in the 3S CCIP, relying more on free-leg momentum than rigid abdominal bracing.

During the flight phase, increasing revolutions demand a more rigid longitudinal axis, driven by the rectus abdominis. In the salchow flight, rectus coactivation jumps from 48.7% in the 2S to 75.6% in the 3S CCII, while left rectus activation climbs to an IITM of 13215 with a PITM of 75.6%. The obliques mirror this core locking mechanism in the air; the left obliquus PITM reaches its study maximum of 80.1% in the 3S with an IITM of 14833 and remains elevated at 80.4% in the 3LO.

During the landing phase, the multi-rotational momentum of triple jumps requires a violent checking response from the lateral walls upon impact. In the loop landing, obliquus coactivation climbs from 72.6% in the 2LO to a study-maximum 88.2% in the 3LO CCII, characterized by an ultra-rapid left obliquus onset peaking at just 0.013 s with an IITM of 6456. At the same time, the rectus wall transitions into a highly lateralized protector of the landing hip during the 3LO, where the left-side activity doubles the right side, reaching a left IITM of 5725 and PITM of 28.6% compared to a right IITM of 3260 and PITM of 13.1%.

3.4 Rotation and Air Time

The analyzed data, as summarized in Table 6, shows that the 3S achieved the highest median values with an air time of 0.55 s and a rotation speed of 1569 °/s. In contrast, the 1A recorded the lowest median values at 0.49 s and 945 °/s. Among double jumps, the 2A reached an air time of 0.53 s and a speed of 1433 °/s, followed by the 2S at 0.53 s and 1106 °/s, and the 2LO at 0.50 s and 1083 °/s. Finally, the 3LO was characterized by a median air time of 0.53 s and a rotation speed of 1422 °/s.

Table 6: Median values of air time and rotation speed for analyzed jumps.

Jump Type	**Air Time (s)**	**Rotation Speed (°/s)**
1A	0,49	945
2A	0,53	1433
2S	0,53	1106
3S	0,55	1569
2LO	0,50	1083
3LO	0,53	1422

Kinematic data (Tab. 6) provide a baseline to understand the neuromuscular demands of different jump difficulties. While air time remained relatively stable, ranging from 0.49 s (1A) to 0.55 s (3S), the rotation speed increased between single and double (double and triple) variations.

This mechanical shift is directly correlated with the EMG patterns observed in the preceding sections 3.1, 3.3 and 3.2. The transition from double to triple jumps (e.g., 2S to 3S or 2LO to 3LO) did not rely on significantly prolonged flight phases, but rather on an increase in IITM of the core muscles. Specifically, the 3S achieved the highest median rotation speed (1569 °/s), which corresponds to the sharpest rise in left-side obliquus externus activation during the flight phase (PITM 62.8% compared to 80.1% in 2S). This suggests that stabilization of a high-velocity rotational axis is achieved through increased muscular tension rather than flight duration.

Furthermore, a comparison between the 2A and 3LO reveals that despite similar rotation speeds (≈1433–1422 °/s), their core activation strategies differ based on the jump's entry mechanism. The 2A, characterized by a forward takeoff, reached its physiological peak during the preparation phase (obliquus IITM ≈ 9900), whereas the 3LO required its highest core synchronization during the landing phase, where obliquus coactivation reached 88.2% CCII to stabilize the longitudinal axis. These findings demonstrate that the core

musculature acts as a dynamic compensator that shifts its activation timing—either for torque generation in preparation or for rigid bracing during landing—depending on the specific mechanical requirements of the jump type.

4 Discussion

Table 7: Summary of figure skating biomechanical studies.

Author (Year)	Main Focus	Methodology	Key Result
Moessing et al. [1] (2025)	IMU placement for jump classification	5 IMUs + video (n=58)	Best placement at ankles (98% acc.); wrist worst.
Panfili et al. [2] (2022)	Wearable system for jump detection	ToF sensors + back-mounted gyroscope	97–99% acc. in height measurement (20 cm threshold).
Bruening et al. [3] (2018)	Wearable IMU jump monitor	IMU algorithms + high-speed video	Identified 39 of 41 multi-revolution routine jumps.
Pantoja et al. [4] (2014)	Roller skating multi-jump comparison	EMG (lower limbs) + laser sensors	Multi-rotational jumps require longer muscle activity.
Koga et al. [5] (2025)	Muscle activity in axel jumps	EMG (5 lower limb muscles) + cameras	Higher rotations correlate with increased vertical velocity.
Yamaguchi et al. [6] (2025)	Angular momentum during jumps	3D MA (n=7)	Trunk holds max momentum; arms transfer swing.
Shi et al. [7] (2020)	Kinematics of flip jumps (1S, 2S, 3S)	5 IMUs (1 subject, multiple trials)	Triple jumps require tighter flight prep control at takeoff.
Bingül et al. [8] (2017)	Core training impact on jump kinematics	8-week core program + pre/post recordings	Increased vertical jump capacity; no kinematic differences for toe loops.
Hara et al. [9] (2024)	3D blade reaction forces on ice	3 wearable force plates + validation plate	Captured vertical GRF and moments during skating.
Li et al. [10] (2024)	Advanced biomechanical human model	Video MoCap (n=4)	Hip-knee coordination is critical for landing stability.
Helesic and Lehnert [11] (2024)	Score prediction via physical tests	Principal component + regression vs. ISU scores	Sprint and horizontal jump strength strongly predict scores.
Mochida et al. [12] (2023)	Core training impact on jump kinematics	High-speed cameras (pre/post training)	Core training altered loop takeoff angle and length.
Hirosawa et al. [13] (2023)	Predictive jump scoring model	Predictive model + eye-tracking + kinematics	Max prediction acc. achieved by combining kinematics and judges' gaze.
Hirosawa et al. [14] (2022)	Correlation of physical params and scores	Video Ice Scope (30 jumps)	Horizontal distance and distance-to-height ratio correlate with higher scores.
Present study	Core muscle activation across 3 jump types at 2 difficulty levels	Torso ACC + bilateral EMG + skate IMUs (n=12)	Shift from right-side core dominance in prep to left-side in flight.

Note: IMU = inertial measurement unit; ToF = time-of-flight; EMG = electromyography; ACC = accelerometer; GRF = ground reaction forces; 3D MA = 3D motion analysis; MoCap = motion capture; ISU = International Skating Union; acc. = accuracy; params = parameters; n = number of subjects; m. = musculus, ext. = externus, abd. = abdominis.

The results of this study provide unique insight into the EMG activity of the core stabilization system during figure skating jumps. By quantifying the activation patterns of the primary abdominal muscles across different technical phases, this research establishes a foundational framework for understanding how the human torso manages the extreme rotational and gravitational demands of multi-revolution elements. Moreover, these empirical data bridge a significant gap in the current literature (Tab. 7), shifting the focus

from lower-limb kinematics to the underlying neuromuscular mechanisms of the trunk that are vital for both athletic performance and long-term injury prevention in young skaters.

Throughout all jump phases, the m. obliquus externus generally exhibited higher percentage activation (%ITM) than the m. rectus abdominis. This finding underscores that figure skating jumps are primarily rotational movements rather than flexion ones. While the rectus abdominis functions largely as a postural stabilizer to prevent spinal collapse, the obliquus externus serves as the primary engine for generating and controlling rotational velocity and stabilizing the pelvis against multi-directional forces.

Regarding the preparation phase, a consistent trend of right-side dominance was observed, particularly in the m. obliquus externus. For all subjects (who performed counter-clockwise rotations), the preparation phase is characterized by an eccentric "loading" of torque. The right m. obliquus externus exhibits higher activation, as it facilitates the initiation of rotational momentum and stabilizes the pelvis against the takeoff leg. Upon takeoff, dominance shifts to the left side (concentric contraction) to "close" the body into a tight rotational axis.

The exceptionally high CCII oblique values during the landing phase (exceeding 88% for 2S and 3LO) indicate a bracing mechanism. To protect the spine and prevent loss of balance, the neuromuscular system responds with a massive simultaneous contraction of all core components. This bilateral symmetry is crucial for the safe absorption of impact energy and the immediate stabilization of the vertical axis required for a clean exit from the jump.

Significant increases in IITM values for the m. obliquus externus were recorded in triple jumps (3S, 3LO) compared to double jumps, despite the flight time being only slightly longer (e.g., 0.50 s for 2LO vs. 0.53 s for 3LO). This disparity suggests that the higher integrated activity is not a function of duration but rather intensity of contraction. As the rotation speed increases from $\approx 1083^\circ/s$ to $\approx 1422^\circ/s$, the core musculature must generate substantially higher tension to overcome deforming forces and maintain a rigid vertical axis.

Despite these insights, several limitations must be acknowledged. The study cohort consisted exclusively of adolescent female athletes, as the project design and the approved institutional ethics committee protocol were specifically limited to this demographic. Consequently, these findings serve as a pilot study and may not be fully generalizable to male skaters or elite adult professionals due to physiological differences in muscle mass and center of gravity; however, expanding the cohort to these populations will be the subject of future follow-up research. Furthermore, the analysis focused only on the superficial abdominal muscles, leaving the roles of deep stabilizers and the erector spinae underexplored. The cold environment of the ice rink also presents technical challenges, as it can affect electrode-skin impedance. While the %ITM normalization method is robust, it remains sensitive to the participant's maximum effort and fatigue levels on the day of testing. Finally, although IMU sensors provided high-precision markers, phase segmentation required manual verification in the cases of signal noise, introducing a minor degree of human error.

Another limitation of the present study lies in the preprocessing pipeline of the raw EMG signals, specifically the absence of an initial high-pass filter prior to the amplitude envelope extraction. Although the subsequent 4th-order low-pass Butterworth filter with a 6 Hz cutoff frequency effectively eliminated high-frequency noise and 50 Hz power-line interference, it was unable to remove low-frequency baseline wander caused by mechanical movement artifacts (e.g., electrode-skin shifting during rapid rotations and impact). Because the full-wave rectification was applied to a signal containing these minor baseline shifts, the calculated peak global maximum—used as the 100% reference for inter-trial normalization—may have been slightly overestimated due to mechanical impacts rather than purely electrochemical muscle activity. Consequently, this might introduce a minor non-linear shift in the PITM and IITM. However, since the data were normalized using intra-subject and trial-specific reference points within identical measurement series, this systemic variation is highly consistent across trials and does not compromise the validity of the observed relative trends in bilateral muscle coactivation.

The findings of this study open up several questions for future research, particularly in expanding the physiological scope of trunk analysis. A primary objective for studies is the inclusion of the posterior chain,

specifically the m. erector spinae. While the abdominal muscles provide anterior and lateral stability, the back musculature is essential to resist the forward trunk lean often caused by the intense impact forces during landing. Measurement of dorsal muscle groups would provide a complete 360-degree profile of the core, allowing researchers to calculate the true spinal compression and stability ratios during high-velocity rotations.

5 Conclusion

This study provides a comprehensive characterization of core muscle activation during multi-revolution figure skating jumps, establishing that the m. obliquus externus acts as the primary engine for rotational control. The distinct shift from right-side dominance during preparation to left-side contraction in flight highlights the precise bilateral coordination required for counter-clockwise spins. Furthermore, the massive co-contraction recorded during landing confirms a neuromuscular bracing mechanism that stabilizes the vertical axis and protects the spine from impact forces. The comparison between difficulty levels reveals that transitioning from double to triple jumps demands a significant increase in muscle contraction intensity, rather than duration, to withstand rotational velocities.

As a pilot study limited to adolescent female athletes according to the approved ethics protocol, these findings lay the foundational framework for future research. Subsequent studies should expand the demographic cohort to include male and elite adult skaters to enhance generalizability. Additionally, incorporating the posterior chain—specifically the m. erector spinae, will provide a complete 360-degree profile of core functionality, crucial for optimizing training and injury prevention in figure skating.

References

[1] Tyler Moessing et al. "Sensor Placement for Jump Classification in Sub-Elite Figure Skating". In: *Proceedings of the First Annual Conference on Human-Computer Interaction and Sports*. Enschede Netherlands: ACM, Nov. 2025, pp. 1–7. ISBN: 979-8-4007-1428-3. DOI: 10.1145/3749385.3749404. URL: https://dl.acm.org/doi/10.1145/3749385.3749404 (visited on 03/30/2026).

[2] Antonio Panfili, Alvise Spanò, and Agostino Cortesi. "A Wearable System for Jump Detection in Inline Figure Skating". In: *Sensors* 22.4 (Feb. 2022), p. 1650. ISSN: 1424-8220. DOI: 10.3390/s22041650. URL: https://www.mdpi.com/1424-8220/22/4/1650 (visited on 03/30/2026).

[3] Dustin A. Bruening et al. "A Sport-Specific Wearable Jump Monitor for Figure Skating". In: *PLOS ONE* 13.11 (Nov. 21, 2018). Ed. by Bijan Najafi, e0206162. ISSN: 1932-6203. DOI: 10.1371/journal.pone.0206162. URL: https://dx.plos.org/10.1371/journal.pone.0206162.

[4] Patrícia Dias Pantoja et al. "Neuromuscular Responses of Elite Skaters During Different Roller Figure Skating Jumps". In: *Journal of Human Kinetics* 41.1 (July 2014), pp. 23–32. ISSN: 1899-7562. DOI: 10.2478/hukin-2014-0029. URL: https://johk.pl/?p=2887 (visited on 03/30/2026).

[5] Ami Koga et al. "Lower Limb Biomechanical Differences between Jumps with Different Number of Rotations in Youth Figure Skaters". In: *Frontiers in Bioengineering and Biotechnology* 13 (Sept. 2025), p. 1606817. ISSN: 2296-4185. DOI: 10.3389/fbioe.2025.1606817. URL: https://www.frontiersin.org/articles/10.3389/fbioe.2025.1606817/full (visited on 03/30/2026).

[6] Mizuki Yamaguchi and Shinji Sakurai. "Comparisons of Angular Momentum at Takeoff in Six Types of Jumps in Women's Figure Skating". In: *Frontiers in Sports and Active Living* 7 (Aug. 2025), p. 1597598. ISSN: 2624-9367. DOI: 10.3389/fspor.2025.1597598. URL: https://www.frontiersin.org/articles/10.3389/fspor.2025.1597598/full (visited on 03/30/2026).

[7] Yuchen Shi, Atsushi Ozaki, and Masaaki Honda. "Kinematic Analysis of Figure Skating Jump by Using Wearable Inertial Measurement Units". In: *The 13th Conference of the International Sports Engineering Association*. The Conference of the International Sports Engineering Association. MDPI, June 15, 2020, p. 124. DOI: 10.3390/proceedings2020049124. URL: https://www.mdpi.com/2504-3900/49/1/124.

[8] B. Bingül et al. "The Impact of Core Training in Figure Skating on the Lower Extremity Kinematics of Loop and Toe Loop Jumps". In: *International Journal of Scientific Research* 6.11 (2017), pp. 36–38. ISSN: 2277-8179. DOI: 10.36106/ijsr.

[9] Yuse Hara et al. "Wearable System for Measuring Three-Dimensional Reaction Forces and Moments Using Six-Axis Force Sensors during Skating". In: *Journal of Biomechanical Science and Engineering* 19.4 (2024), pp. 24-00093-24–00093. ISSN: 1880-9863. DOI: 10.1299/jbse.24-00093. URL: https://www.jstage.jst.go.jp/article/jbse/19/4/19_24-00093/_article (visited on 04/17/2026).

[10] Han Li and Lianzhong Cao. "ANALYSIS AND SIMULATION OF HUMAN DYNAMICS IN FIGURE SKATING SPORTS". In: *Journal of Mechanics in Medicine and Biology* 24.08 (Oct. 2024), p. 2440054. ISSN: 0219-5194, 1793-6810. DOI: 10.1142/S0219519424400542. URL: https://www.worldscientific.com/doi/10.1142/S0219519424400542 (visited on 03/30/2026).

[11] Jiri Helesic and Michal Lehnert. "Explosive Strength and Speed as Potential Determinants of Success in Youth Figure Skating Competitions". In: *Applied Sciences* 14.24 (Dec. 2024), p. 11861. ISSN: 2076-3417. DOI: 10.3390/app142411861. URL: https://www.mdpi.com/2076-3417/14/24/11861.

[12] Miho Mochida, Boyang Jin, and Yudong Zhang. "EFFECTS OF STRETCHING TRAINING ON LOWER LIMB EXPLOSIVE STRENGTH IN FIGURE SKATING ATHLETES". In: *Revista Brasileira de Medicina do Esporte* 29 (2023), e2022_0350. ISSN: 1806-9940, 1517-8692. DOI: 10.1590/1517-8692202329012022_0350. URL: http://www.scielo.br/scielo.php?script=sci_arttext&pid=S1517-86922023000100395&tlng=en (visited on 03/30/2026).

[13] Seiji Hirosawa et al. "Action Quality Assessment Model Using Specialists' Gaze Location and Kinematics Data—Focusing on Evaluating Figure Skating Jumps". In: *Sensors* 23.22 (Nov. 2023), p. 9282. ISSN: 1424-8220. DOI: 10.3390/s23229282. URL: https://www.mdpi.com/1424-8220/23/22/9282.

[14] Seiji Hirosawa, Michiko Watanabe, and Yoshimitsu Aoki. "Determinant Analysis and Developing Evaluation Indicators of Grade of Execution Score of Double Axel Jump in Figure Skating". In: *Journal of Sports Sciences* 40.4 (Feb. 2022), pp. 470–481. ISSN: 0264-0414, 1466-447X. DOI: 10.1080/02640414.2021.1997407. URL: https://www.tandfonline.com/doi/full/10.1080/02640414.2021.1997407 (visited on 03/30/2026).

[15] Wayne J. Albert and Doris I. Miller. "Takeoff Characteristics of Single and Double Axel Figure Skating Jumps". In: *Journal of Applied Biomechanics* 12.1 (Feb. 1996), pp. 72–87. ISSN: 1065-8483, 1543-2688. DOI: 10.1123/jab.12.1.72. URL: https://journals.humankinetics.com/view/journals/jab/12/1/article-p72.xml (visited on 04/27/2026).

[16] Psycharakis Taylor. *A Pilot Study on Electromyographic Analysis of Single and Double Revolution Jumps in Figure Skating*. DOI: 10.3316/informit.857648217212634. URL: https://search.informit.org/doi/epdf/10.3316/informit.857648217212634 (visited on 04/27/2026).

[17] Yu Okubo et al. "Abdominal Muscle Activity during a Standing Long Jump". In: *The Journal of Orthopaedic and Sports Physical Therapy* 43.8 (Aug. 2013), pp. 577–582. ISSN: 1938-1344. DOI: 10.2519/jospt.2013.4420.

[18] Pablo Ortega-Auriol, Thor Besier, and Angus J. C. McMorland. "Effect of Surface Electromyography Normalisation Methods over Gait Muscle Synergies". In: *Journal of Electromyography and Kinesiology* 80 (Feb. 2025), p. 102968. ISSN: 1050-6411. DOI: 10.1016/j.jelekin.2024.102968. URL: https://www.sciencedirect.com/science/article/pii/S1050641124001123 (visited on 04/28/2026).

[19] Gordon G. Sleivert and Howard A. Wenger. "Reliability of Measuring Isometric and Isokinetic Peak Torque, Rate of Torque Development, Integrated Electromyography, and Tibial Nerve Conduction Velocity". In: *Archives of Physical Medicine and Rehabilitation* 75.12 (Dec. 1994), pp. 1315–1321. ISSN: 0003-9993. DOI: 10.1016/0003-9993(94)90279-8. URL: https://www.sciencedirect.com/science/article/pii/0003999394902798 (visited on 04/27/2026).

[20] Thor F. Besier, David G. Lloyd, and Timothy R. Ackland. "Muscle Activation Strategies at the Knee during Running and Cutting Maneuvers:" in: *Medicine & Science in Sports & Exercise* 35.1 (Jan. 2003), pp. 119–127. ISSN: 0195-9131. DOI: 10.1097/00005768-200301000-00019. URL: http://journals.lww.com/00005768-200301000-00019 (visited on 04/27/2026).